Chemistry–A European Journal
Research Article
doi.org/10.1002/chem.202201385
Chemistry Europe
European Chemical Societies Publishing
www.chemeurj.org

Photochemical Synthesis of the Bioactive Fragment of Salbutamol and Derivatives in a Self-Optimizing Flow Chemistry Platform

Romaric Gérardy,[a] Anirudh M. K. Nambiar,[a] Travis Hart,[a] Prajwal T. Mahesh,[a] and Klavs F. Jensen*[a]

Abstract: The implementation of self-optimizing flow reactors has been mostly limited to model reactions or known synthesis routes. In this work, a self-optimizing flow photochemistry platform is used to develop an original synthesis of the bioactive fragment of Salbutamol and derivatives. The key photochemical steps for the construction of the aryl vicinyl amino alcohol moiety consist of a C–C bond forming reaction followed by an unprecedented, high yielding (>80%), benzylic oxidative cyclization.

β_2-adrenoceptor agonists are a class of medicines used mainly in the treatment of asthma and chronic obstructive pulmonary disease.[1] Representatives of this class include Salbutamol and Salmeterol, which are sold as racemates, and were both listed in the Top 200 Drugs by sales in the 2010s.[1] Salbutamol is notably featured on the World Health Organization's List of Essential Medicines.[2]

The common bioactive fragment of Salbutamol and Salmeterol is an aryl vicinyl amino alcohol (Figure 1a), the synthesis of which is potentially challenging due to high hydrophilicity of the reaction intermediates and product.[3] Researchers at GSK have designed a strategy that instead utilizes surrogate *(R)*-**1** as convenient entry for the synthesis of *(R)*-Salmeterol and other β_2-adrenoceptor agonists.[4] The method described for the preparation of *(R)*-**1** is a lengthy 9-step synthesis.[4a,5]

In this context, the development of a shorter synthesis of racemic **1** prompted our interest. Inspired by prior studies[6,7] (Figure 1b), we envisioned that the central 2-oxazolidinone could be installed early in the process (Figure 1c). To reduce the experimental burden associated with the development of our methodology, we decided to deploy these steps in a self-optimizing flow photochemistry platform. Photochemical reactions benefit from the higher surface-area-to-volume ratios and shorter radial length scales characteristic of continuous flow tubular reactors. These features enable greater photon penetration (due to the Beer-Lambert law) and more uniform irradiation of the reaction mixture.[8] Flow reactor hardware can be combined with control software, automation scripts, process analytical technology (PAT),[9] as well as optimization algorithms that use prior data to propose new reaction conditions to try, in order to maximize an objective (e.g., yield) with fewer experiments.[9c,10] This integration has enabled "self-optimizing" flow chemistry platforms (SOFCP) that assist a chemist's work-

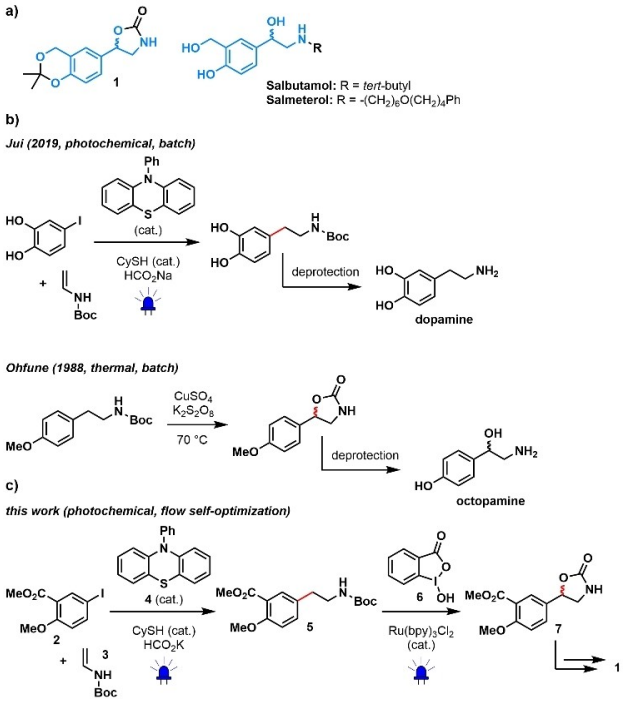

Figure 1. (a) Structures of β_2-adrenoceptor agonists and their protected bioactive fragment **1**. (b) Previous approaches towards bioactive amines/amino alcohols. (c) Photochemical synthesis presented in this work.

[a] *Dr. R. Gérardy, Dr. A. M. K. Nambiar, T. Hart, P. T. Mahesh, Prof. Dr. K. F. Jensen*
Department of Chemical Engineering
Massachusetts Institute of Technology
77 Massachusetts Avenue, Cambridge, MA 02139 (USA)
E-mail: kfjensen@mit.edu

Supporting information for this article is available on the WWW under https://doi.org/10.1002/chem.202201385

flow by automating routine tasks such as experiment design, execution, and analysis. However, the application of SOFCP has been mostly limited to model chemistries[11] or known reaction routes.[12]

Our investigation commenced with initial photochemical batch experiments that served two purposes: (1) identifying flow-compatible conditions and (2) isolating reaction (side-)products to calibrate the HPLC upon which our self-optimization would rely.

The first reaction consisted of a C–C bond forming reaction between an aryl iodide and *tert*-butyl vinylcarbamate (**3**), triggered by blue light irradiation of photocatalyst **4** in the presence of cyclohexanethiol (**CySH**) as hydrogen atom transfer catalyst (Figure 1c). The conditions proposed in the original paper[6] (0.1 M of aryl iodide in DMSO/H_2O 95:5, 3 equiv. of HCO_2Na) were successful but flow-incompatible due to the insolubility of HCO_2Na. Alternatively, utilization of HCO_2K (1.25 equiv) in DMSO/H_2O 9:1 gave a homogeneous reaction without affecting the yield (Supporting Information).

In the second reaction, a benzylic cation is generated on the substrate and reacts intramolecularly with the carbonyl of the neighboring *tert*-butoxycarbonyl (Boc) protecting group, eventually forming the target 2-oxazolidinone scaffold along with a *tert*-butyl cation (Supporting Information for details of the proposed mechanism). The original method[7] proceeds by thermal activation of $K_2S_2O_8$ and $CuSO_4$, and was successfully utilized in other advanced syntheses.[13] In the pursuit of a milder method that would rather rely on photochemical activation, we envisioned that the conditions described by others for the hydroxylation of benzylic C–H bonds[14] could trigger the reaction of interest. Initial batch experiments (Supporting Information) thus consisted of blue light irradiation of $Ru(bpy)_3Cl_2$ (5 mol%) in the presence of the substrate and 2 equiv. of 2-iodosobenzoic acid (**6**) (Figure 1c). These preliminary tests indicated that the substrate's phenol required a methyl protecting group for the reaction to proceed, hence imposing the use of aryl iodide **2** in the first step. The reaction was also initially flow-incompatible, due to the insolubility of 2-iodosobenzoic acid (**6**) in hexafluoroisopropanol (HFIP)/water. Other solvents did not solve the issue and it was decided to use **6** at its limit of solubility in hexafluoroisopropanol (HFIP)/H_2O 9:1 (0.065 M).

The hardware of the SOFCP used in this study (Figure 2 and Supporting Information) is detailed in previous papers.[12c,15] Briefly, four feedstock solutions (substrate, reactant, catalyst and pure solvent) were pumped using VICI M6HP pumps into a 0.125 mL active mixing chamber equipped with a stir bar, before entering a 1 mL coiled tubular reactor (PFA tubing, 1/32″ ID, 1/16″ OD) where irradiation occurred. For this purpose, we designed an attachable module consisting of 16 LEDs (450 nm maximum emission) mounted with fans and a heat sink for heat dissipation. The photon flux directed towards the reactor was characterized by spectroradiometry and actinometry, which suggested intense and efficient irradiation (Supporting Information). The reactor was maintained at 40 °C throughout the optimization campaigns to ensure a stable temperature profile over time. After exiting the reactor, the reaction medium

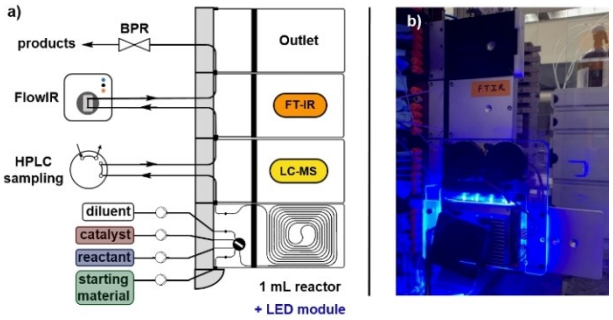

Figure 2. (a) Process diagram of the SOFCP utilized for the optimization of photochemical steps. The LED module is omitted for clarity. The arrows correspond to the direction of the flow. (b) Picture of the SOFCP with the LED module.

entered two analytical modules for quantitative (HPLC) and qualitative (FTIR) monitoring, before being redirected towards a Zaiput back pressure regulator (BPR) and eventually exiting the platform. This configuration was used for the optimization of both photochemical steps.

Concerning the optimization algorithm, we used the Dragonfly Bayesian optimization package which is available open-source in Python (details in Supporting Information).[16] The algorithm employs a Gaussian process surrogate model to mathematically describe the relationship between input variables and objective function. After fitting the model to initialization data, the algorithm iteratively proposes a new reaction condition to try, based on a combination of where the objective value is expected to be high (exploitative strategy) and where model uncertainty is high (explorative strategy) to increase the likelihood of identifying a global optimum.

The search space for the self-optimization of the first step consisted of 3 continuous variables: (a) the equivalents of alkene **3** (1–3 equiv), (b) the loading of co-catalyst **CySH** (1–50 mol%) and the residence time (5–30 min). The yield of product **5** was defined as the objective of the optimization, since it would capture both conversion of substrate **2** and selectivity for **5** over side-product **SP-5** (Figure 3a).[6] The self-optimization campaign was initiated with 6 experiments generated by Latin hypercube sampling, spanning most of the search space (1.2–2.7 equiv. of **3**, 10–45 mol% of **CySH**, 5–25 min residence time). These initial experiments afforded 14.4-38.4% yields (Figures 3b,c and Supporting Information for detailed values of conversion and yield), with **SP-5** and unconverted **2** closing the mass balance of the reaction. In the subsequent part of the optimization, the algorithm explored higher equivalents of **3** (typically 2.5–3 equiv) and longer residence times (typically 20–30 min). Regarding the loading of **CySH**, the algorithm initially maintained its exploration of the whole range (4–50 mol%) in experiments 7–13, and then refined the search to 44–50 mol% in experiments 14–19. In this latter upper corner of the search space, **5** yield fluctuated between 39.9 and 41.3%. Eventually, the algorithm explored intermediate **CySH** loadings (26–28 mol%) in experiments 20 and 21, which gave the highest yields of the campaign (45.3

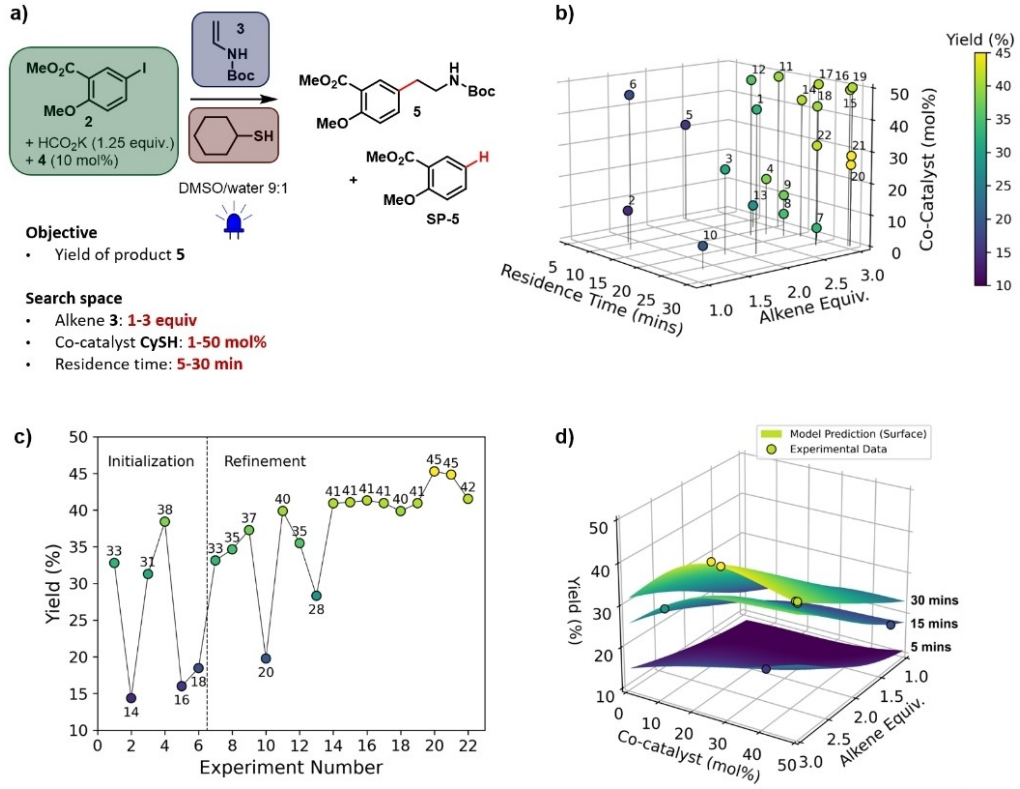

Figure 3. Self-optimization of the photochemical C–C bond forming reaction. a) Details of the chemistry. The colored frames represent the different feedstock solutions utilized in the platform (see Figure 2 and Supporting Information). Other parameters: T = 40 °C, P = 75 psi. Yields were determined by HPLC analysis using biphenyl as internal standard. b) Yields obtained within the search space. The labels represent experiment number. c) Evolution of **5** yield as a function of the experiment number. The color and labels both represent yield. d) Yield response surfaces generated using the algorithm's Gaussian process mathematical model fitted to experimental data.

and 44.8%, respectively). As such, with no *a priori* knowledge of the chemistry on the algorithm side, our optimization gave similar conclusions to those of Jui and coworkers.[6] That is, (a) an intermediate loading of **CySH** is advantageous since the co-catalyst is detrimental to conversion and selectivity at low and high loadings, respectively and (b) a large excess of alkene is beneficial to the selectivity with little to no effect on the conversion. The latter statement is supported by comparison of the results of experiment 7 with those of experiment 10: with similar residence times (25.3 and 26.9 min, respectively) and **CySH** loadings (4.1 and 7.1 mol%, respectively), but more than a twofold increase of alkene **3** equivalents (2.88 and 1.25, respectively), the conversion was slightly lower (66.5% and 71.7%, respectively), but selectivity was dramatically enhanced (49.8% and 27.6%, respectively). Our results also suggest that while being stuck in a local maximum in experiments 14–19, the algorithm eventually found the global maximum of the search space (Figure 3c). This first self-optimization campaign of 22 experiments took 28 h. The algorithm's Gaussian process mathematical model fitted to the experimental data was utilized to generate yield response surfaces (Figure 3d) that illustrate the aforementioned trends (i.e., high alkene equivalents and intermediate co-catalyst loadings are optimal).

Likewise, 3 continuous variables were considered for the optimization of the second step: (a) the equivalents of the oxidant **6** (1–2 equiv), (b) the loading of photocatalyst $Ru(bpy)_3Cl_2$ (1–15 mol%) and the residence time (5–25 min). Similarly to step 1, the yield of product **7** was defined as the objective of the optimization (reflecting the conversion of substrate **5** and the selectivity for **7** over side-product **SP-7**) (Figure 4a).

Our optimization commenced with 6 initial experiments that covered most of the search space: from 1.12 to 1.83 equiv. of **6**, from 3.6 to 14.2 mol% of ruthenium photocatalyst, and from 6 to 24 min of residence time. This unprecedented photochemical reaction directly afforded an excellent yield (80.6%) in the first experiment of the campaign, using 1.83 equiv. of hypervalent iodine **6**, 13.2 mol% of photocatalyst, and a residence time of 19.5 min. The remaining initial experiments yielded variable amounts of **7** (between 5.2 and 58.1% yield), with unconverted **5** and side-product **SP-7** closing the mass balance (Figure 4b,c and Supporting Information for detailed values of conversion and yield). Following initialization, the algorithm rapidly converged towards the highest yield of the optimization (83.5%) in experiment 10, corresponding to the boundary conditions of the search space (highest molar ratio of **6**, highest loading of photocatalyst and longest residence time) (Figure 4b). Even though experiment 10 gave the highest yield of product **7**, experiment 1 could be considered as the optimized conditions of the search space,

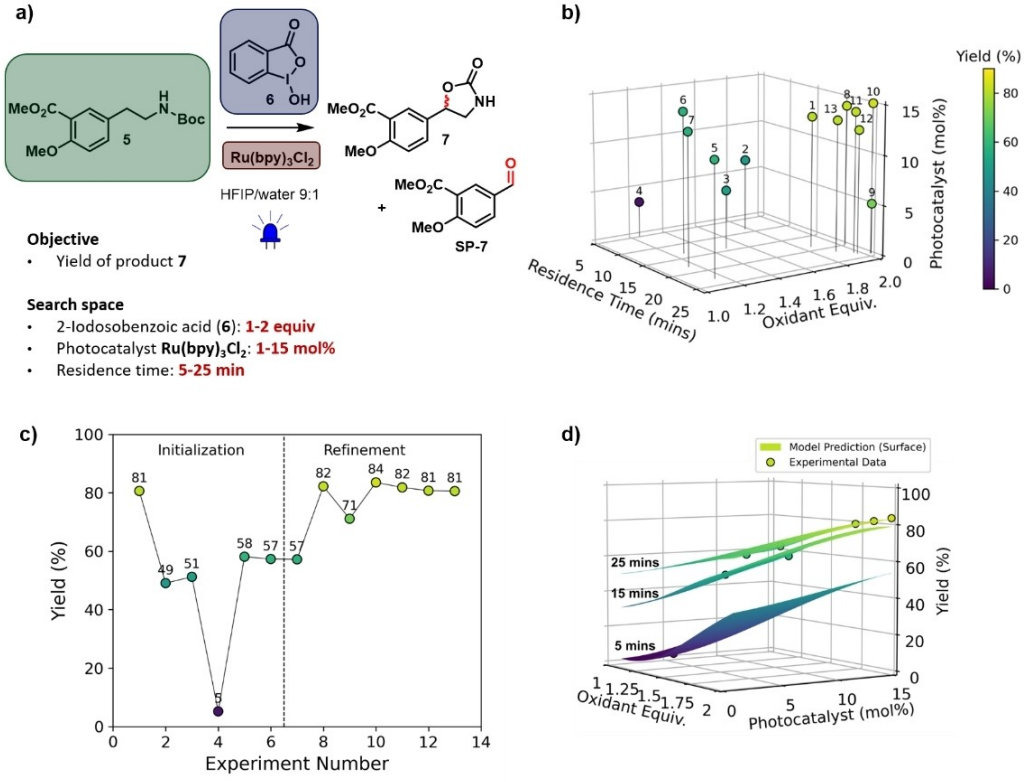

Figure 4. Self-optimization of the photochemical benzylic oxidative cyclization. a) Details of the chemistry. The colored frames represent the different feedstock solutions utilized in the platform (see Figure 2 and Supporting Information). Other parameters: T = 40 °C, P = 50 psi. Yields were determined by HPLC analysis using biphenyl as internal standard. b) Yields obtained within the search space. The labels represent experiment number. c) Evolution of **7** yield as a function of the experiment number. The color and labels both represent yield. d) Yield response surfaces generated using the algorithm's Gaussian process mathematical model fitted to experimental data.

since they afforded an excellent yield as well, while slightly reducing resources consumption. This second self-optimization campaign of 13 experiments took 14 h. In Figure 4d, response surfaces generated using the algorithm's Gaussian process model show how yield varies across the search space.

The subsequent reactions for the transformation of **7** into final product **1** are standard in the literature and were incompatible with our SOFCP (cryogenic conditions and/or involving solids). As such, it was decided to run them in batch without thorough optimization (Supporting Information).

The methyl protecting group of **7** was first cleaved into the corresponding phenol with BBr_3 at −78 °C in CH_2Cl_2 (62 % yield). The presence of a phenol adjacent to the methyl ester enabled the reduction of the latter to proceed by refluxing the substrate in THF in the presence of $NaBH_4$.[17] The resulting crude 2-hydroxybenzyl alcohol was highly water-soluble and was hence eventually protected, without intermediate isolation, into final compound **1** with acetone/2,2-dimethoxypropane 1:1 and a catalytic amount of *p*-toluenesulfonic acid at room temperature. These last steps (ester reduction and ketal protection) afforded target compound **1** in 58 % isolated yield as a stable lipophilic solid, the NMR data of which matched those of the literature (Supporting Information).[4a]

In conclusion, the results presented herein disclose an original route that is shorter than conventional methods for the preparation of the bioactive fragment of Salbutamol and derivatives. The first C–C bond forming reaction and second benzylic oxidative cyclization step were thoroughly optimized in a SOFCP. In the first campaign, our system identified, with no *a priori* knowledge of the chemistry, trends that were identical to those of previous literature. The second unprecedented photochemical reaction gave excellent results, and the platform found these optimized conditions in only 10 experiments. Once initiated, the automated system performed each campaign unattended overnight, which significantly reduced manual effort during reaction optimization. Overall, our work discloses a concrete example of route development accelerated by self-optimizing flow reactors.

Acknowledgements

The authors express their gratitude to Brooke Jin for helping fabricate the LED module. R.G. thanks the Belgian American Educational Foundation for his postdoctoral fellowship. This work was supported by the DARPA Make-It and Accelerated Molecular Discovery programs under contracts ARO W911NF-16-2-0023 and HR00111920025, respectively.

Conflict of Interest

The authors declare no conflict of interest.

Data Availability Statement

The data that support the findings of this study are available in the supplementary material of this article.

Keywords: automation · flow chemistry · photochemistry · self-optimization · synthetic methods

[1] R. Vardanyan, V. Hruby, in *Synthesis of Best-Seller Drugs*, Academic Press, **2016**, pp 357–381.
[2] World Health Organization Model Lists of Essential Medicines, https://www.who.int/medicines/publications/essentialmedicines/en/, (Accessed on Feb. 19, 2022).
[3] A. Vanoost, L. Petit, *Tetrahedron Lett.* **2020**, *61*, 152126.
[4] a) D. M. Coe, R. Perciaccante, P. A. Procopiou, *Org. Biomol. Chem.* **2003**, *1*, 1106–1111; b) P. A. Procopiou, V. J. Barrett, N. J. Bevan, K. Biggadike, P. R. Butchers, D. M. Coe, R. Conroy, D. D. Edney, R. N. Field, A. J. Ford, S. B. Guntrip, B. E. Looker, I. M. McLay, M. J. Monteith, V. S. Morrison, P. J. Mutch, S. A. Richards, R. Sasse, C. E. Smith, *J. Med. Chem.* **2009**, *52*, 2280–2288; c) P. A. Procopiou, V. J. Barrett, N. J. Bevan, K. Biggadike, P. C. Box, P. R. Butchers, D. M. Coe, R. Conroy, A. Emmons, A. J. Ford, D. S. Holmes, H. Horsley, F. Kerr, A.-M. Li-Kwai-Cheung, B. E. Looker, I. S. Mann, I. M. McLay, V. S. Morrison, P. J. Mutch, C. E. Smith, P. Tomlin, *J. Med. Chem.* **2010**, *53*, 4522–4530; d) P. A. Procopiou, V. J. Barrett, A. J. Ford, B. E. Looker, G. E. Lunniss, D. Needham, C. E. Smith, G. Somers, *Bioorg. Med. Chem.* **2011**, *19*, 6026–6032; e) P. A. Procopiou, V. J. Barrett, K. Biggadike, P. R. Butchers, A. Craven, A. J. Ford, S. B. Guntrip, D. S. Holmes, S. C. Hughes, A. E. Jones, B. E. Looker, P. J. Mutch, M. Ruston, D. Needham, C. E. Smith, *J. Med. Chem.* **2014**, *57*, 159–170.
[5] R. N. Bream, S. V. Ley, P. A. Procopiou, *Org. Lett.* **2002**, *4*, 3793–3796.
[6] A. J. Boyington, C. P. Seath, A. M. Zearfoss, Z. Xu, N. T. Jui, *J. Am. Chem. Soc.* **2019**, *141*, 4147–4153.
[7] K. Shimamoto, Y. Ohfune, *Tetrahedron Lett.* **1988**, *29*, 5177–5180.
[8] N. J. W. Straathof, T. Noël in *Visible Light Photocatalysis in Organic Chemistry*, Wiley-VCH, Weinheim, Germany, **2018**, pp. 389–413.
[9] a) P. Giraudeau, F.-X. Felpin, *React. Chem. Eng.* **2018**, *3*, 399–413; b) P. Sagmeister, R. Lebl, I. Castillo, J. Rehrl, J. Kruisz, M. Sipek, M. Horn, S. Sacher, D. Cantillo, J. D. Williams, C. O. Kappe, *Angew. Chem. Int. Ed.* **2021**, *60*, 8139–8148; *Angew. Chem.* **2021**, *133*, 8220–8229; c) C. Mateos, M. J. Nieves-Remacha, J. A. Rincón, *React. Chem. Eng.* **2019**, *4*, 1536–1544.
[10] C. P. Breen, A. M. K. Nambiar, T. F. Jamison, K. F. Jensen, *Trends Chem.* **2021**, *3*, 373–386.
[11] For examples, see: a) A.-C. Bédard, A. Adamo, K. C. Aroh, M. G. Russell, A. A. Bedermann, J. Torosian, B. Yue, K. F. Jensen, T. F. Jamison, *Science* **2018**, *361*, 1220–1225; b) A. D. Clayton, A. M. Schweidtmann, G. Clemens, J. A. Manson, C. J. Taylor, C. G. Niño, T. W. Chamberlain, N. Kapur, A. J. Blacker, A. A. Lapkin, R. A. Bourne, *Chem. Eng. J.* **2020**, *384*, 123340; c) K. Poscharny, D. C. Fabry, S. Heddrich, E. Sugiono, M. A. Liauw, M. Rueping, *Tetrahedron* **2018**, *74*, 3171–3175.
[12] For examples, see: a) D. Cortés-Borda, E. Wimmer, B. Gouilleux, E. Barré, N. Oger, L. Goulamaly, L. Peault, B. Charrier, C. Truchet, P. Giraudeau, M. Rodriguez-Zubiri, E. Le Grognec, F.-X. Felpin, *J. Org. Chem.* **2018**, *83*, 14286–14289; b) E. Wimmer, D. Cortés-Borda, S. Brochard, E. Barré, C. Truchet, F.-X. Felpin, *React. Chem. Eng.* **2019**, *4*, 1608–1615; c) A. M. K. Nambiar, C. P. Breen, T. Hart, T. Kulesza, T. F. Jamison, K. F. Jensen, *ACS Cent. Sci.* **2022**, DOI: https://pubs.acs.org/doi/10.1021/acscentsci.2c00207m; d) D. E. Fitzpatrick, T. Maujean, A. C. Evans, S. V. Ley, *Angew. Chem. Int. Ed.* **2018**, *57*, 15128–15132; *Angew. Chem.* **2018**, *130*, 15348–15352.
[13] a) J. Toueg, C. R. A. Godfrey, J. E. Wibley, *Synlett* **2010**, 2721–2724; b) S. Shabani, J. M. White, C. A. Hutton, *Org. Lett.* **2019**, *21*, 1877–1880.
[14] G.-X. Li, C. A. Morales-Rivera, F. Gao, Y. Wang, G. He, P. Liu, G. Chen, *Chem. Sci.* **2017**, *8*, 7180–7185.
[15] a) C. W. Coley, D. A. Thomas, J. A. M. Lummiss, J. N. Jaworski, C. P. Breen, V. Schultz, T. Hart, J. S. Fishman, L. Rogers, H. Gao, R. W. Hicklin, P. P. Plehiers, J. Byington, J. S. Piotti, W. H. Green, A. J. Hart, T. F. Jamison, K. F. Jensen, *Science* **2019**, *365*, eaax1566; b) F. Florit, A. M. K. Nambiar, C. P. Breen, T. F. Jamison, K. F. Jensen, *React. Chem. Eng.* **2021**, *6*, 2306–2314.
[16] a) K. Kandasamy, K. R. Vysyaraju, W. Neiswanger, B. Paria, C. R. Collins, J. Schneider, B. Póczos, E. P. Xing, *J. Mach. Learn. Res.* **2020**, *21*, 81; b) B. Paria, K. Kandasamy, B. Póczos, *arXiv preprint*, 2018, arXiv: 1805.12168[cs.LG]; c) GitHub for Dragonfly Bayesian optimization package: https://github.com/dragonfly/dragonfly (Accessed on Feb. 19, 2022).
[17] H. Asakawa, Y. Fukushima, E. Imamiya, Y. Kawamatsu, *Chem. Pharm. Bull.* **1979**, *27*, 522–527.

Manuscript received: May 5, 2022
Accepted manuscript online: May 15, 2022
Version of record online: June 8, 2022